

# Numerical Linked-Cluster Algorithms. II. $t$ - $J$ models on the square lattice

Marcos Rigol

*Department of Physics and Astronomy, University of Southern California, Los Angeles, California 90089, USA*

Tyler Bryant and Rajiv R. P. Singh

*Department of Physics, University of California, Davis, California 95616, USA*

(Dated: February 1, 2008)

We discuss the application of a recently introduced numerical linked-cluster (NLC) algorithm to strongly correlated itinerant models. In particular, we present a study of thermodynamic observables: chemical potential, entropy, specific heat, and uniform susceptibility for the  $t$ - $J$  model on the square lattice, with  $J/t = 0.5$  and  $0.3$ . Our NLC results are compared with those obtained from high-temperature expansions (HTE) and the finite-temperature Lanczos method (FTLM). We show that there is a sizeable window in temperature where NLC results converge without extrapolations whereas HTE diverges. Upon extrapolations, the overall agreement between NLC, HTE, and FTLM is excellent in some cases down to  $0.25t$ . At intermediate temperatures NLC results are better controlled than other methods, making it easier to judge the convergence and numerical accuracy of the method.

PACS numbers: 05.50.+q, 05.70.-a, 75.10.Lp, 05.10.-a

## I. INTRODUCTION

In a recent paper [1] we introduced a linked-cluster algorithm, which we called the numerical linked-cluster (NLC) algorithm, that allows one to obtain temperature-dependent properties of quantum lattice models in the thermodynamic limit from the exact diagonalization of small clusters. A detailed exposition of NLC and its application to quantum spin models on square, triangular, and kagomé lattices has been presented in Ref. [2]. There we have shown that for many spin models and thermodynamic quantities NLC results can be substantially more accurate than HTE and exact diagonalization (ED).

In this paper we discuss how to use NLC to calculate properties of strongly correlated itinerant models. In particular, we study the thermodynamics of the planar  $t$ - $J$  model on the square lattice. This model was introduced by Anderson and others [3, 4] as a means to understanding the microscopic mechanism for high-temperature superconductivity [5, 6]. It is one of the simplest models that allows one to study the interplay between itinerancy of electrons and their spin fluctuations, possibly leading to superconductivity and many other exotic quantum phases [7].

In spite of its simplicity, understanding finite-temperature thermodynamic properties of the  $t$ - $J$  model has proven to be a very challenging task [8]. Quantum Monte Carlo simulations suffer from severe sign problems, which become a major difficulty at low temperatures. The two general approaches that have been commonly used to study this model are ED and HTE. ED studies in which one fully diagonalizes the  $t$ - $J$  Hamiltonian are difficult since they can only be done for very small systems [9, 10], as a consequence of which finite size effects are very large. A more efficient approach to this problem is the finite-temperature Lanczos method (FTLM), which has been developed by Jaklič

and Prelovšek (JP) [11]. Within this approach the full thermodynamic trace is reduced by randomly sampling the eigenstates of the Hamiltonian. This allows one to study larger systems sizes in an unbiased way, but still finite size effects become relevant as the temperature is lowered.

In order to obtain results in the thermodynamic limit one can use high-temperature expansions (HTE) [12, 13, 14, 15]. Within this method the properties of the system are expanded in powers of the inverse temperature  $\beta$  [16, 17]. These expansions, carried out to order  $\beta^N$ , where  $N$  is of order 10, provide accurate numerical results within the radius of convergence of the series. The temperature scale where HTE converges can be rather high for  $t$ - $J$  models. It is typically set by  $t$  when  $t > J$ . Beyond the region of convergence, series extrapolation methods [18] allow one to calculate thermodynamic properties, but their reliability remains uncertain. Because the region of convergence is small in inverse temperature, extrapolations even to temperatures of order  $J$  are more sensitive to the choice of the extrapolation method and variables and hence less reliable than for purely spin models.

Here, we study thermodynamic properties of the  $t$ - $J$  model using NLC. The basic idea is to show with examples the advantages and disadvantages of NLC as compared with FTLM and HTE, and the region of temperatures that within NLC can be accessed for the different observables of interest. The exposition is organized as follows. In Sec. II we introduce the  $t$ - $J$  Hamiltonian and discuss the basic ideas of the NLC calculation for itinerant models. The calculations must be done in the grand canonical ensemble and the change from chemical potential to density must be done numerically. We will show that this works quite well. In the remaining sections we present results for the entropy (Sec. III), the uniform susceptibility (Sec. IV), and the specific heat (Sec. V). The

conclusions are presented in Sec. VI

## II. GRAND CANONICAL NLC

The  $t$ - $J$  Hamiltonian can be written as

$$\mathcal{H} = -t \sum_{\langle i,j \rangle, s} P \left( c_{is}^\dagger c_{j\sigma} + \text{H.c.} \right) P + J \sum_{\langle i,j \rangle} \left( \mathbf{S}_i \cdot \mathbf{S}_j - \frac{1}{4} n_i n_j \right), \quad (1)$$

where  $c_{is}^\dagger$  and  $c_{is}$  are the creation and annihilation operators for an electron with spin  $s = \uparrow, \downarrow$  on a site  $i$ ,  $n_i = \sum_s c_{is}^\dagger c_{is}$  is the density operator,  $P$  is a projection operator to ensure no hopping produces doubly occupied sites, i.e., we assume that the local Coulomb repulsion is very large such that two electrons (with antiparallel spin) cannot be on the same lattice site, and

$$\mathbf{S}_i = \frac{1}{2} \sum_{ss'} c_{is}^\dagger \boldsymbol{\sigma}_{ss'} c_{is'} \quad (2)$$

is the local spin operator ( $\boldsymbol{\sigma}$  are the Pauli matrices). The sums  $\langle i, j \rangle$  in Eq. (1) run over nearest-neighbor sites.

As in the case of spin systems [1, 2], the fundamental basis of our numerical linked cluster expansion, for some extensive property  $P$  of an infinite lattice  $\mathcal{L}$ , is the relation [16, 17]

$$P(\mathcal{L})/N = \sum_c L(c) \times W_P(c), \quad (3)$$

where the left hand side is the value of the property  $P$  per lattice site in the thermodynamic limit. On the right hand side  $L(c)$  is the so-called lattice constant that is the number of embeddings of the cluster  $c$ , per lattice site, in the lattice  $\mathcal{L}$ .  $W_P(c)$  is the weight of the cluster  $c$  for the property  $P$ . The latter is defined recursively by the principle of inclusion and exclusion [16]

$$W_P(c) = P(c) - \sum_{s \subset c} W_P(s), \quad (4)$$

where  $P(c)$  is the property  $P$  calculated for the finite cluster  $c$ . The sum on  $s$  runs over all subclusters of  $c$ . The basic idea of NLC is to calculate  $P$  and  $W_P$  at any temperature by means of an exact diagonalization of each cluster  $c$ .

For itinerant models, it is desirable to control the density in the thermodynamic limit. Within NLC this is achieved by working in the grand canonical ensemble, i.e., by introducing a chemical potential. Hence, in this case

$$P(c) = \frac{1}{Z_c} \text{Tr} \left\{ P \exp \left[ - \left( \mathcal{H} - \mu \sum_i n_i \right) / T \right] \right\}_c \quad (5)$$

In Eq. (5),  $\mu$  denotes the chemical potential,  $T$  is the temperature of the system (we have set the Boltzmann constant  $k_B$  to be unity), and  $Z_c$  is the partition function in each cluster  $c$

$$Z_c = \text{Tr} \left\{ \exp \left[ - \left( \mathcal{H} - \mu \sum_i n_i \right) / T \right] \right\}_c \quad (6)$$

Notice that in Eq. (5) and Eq. (6),  $\text{Tr}$  denotes the grand canonical trace, i.e., we fully diagonalize the  $t$ - $J$  Hamiltonian for all possible fillings in each cluster. This, together with the fact that the Hilbert space is larger (three states per site) for the  $t$ - $J$  model, when compared with 1/2-spin models (with only two states per site) studied in Refs. [1, 2], reduces the size of the largest clusters we can consider here. All results presented in this paper correspond to the site expansion of the square lattice (see Ref. [2] for details) with all clusters up to 10 sites. At zero doping, i.e., the Heisenberg model, we present NLC results considering all clusters with up to 13 sites [1, 2]. In addition, throughout this work we examine two values of the parameter  $J/t$ :  $J/t = 0.5$  as in the HTE studies of Ref. [13], and  $J/t = 0.3$  as in the FTLM studies of Refs. [8, 11], to both of which we compare some of our results.

For itinerant models, the first quantity one needs to evaluate within NLC is the density. This is because one is, in general, interested in the behavior of thermodynamic observables as a function of the temperature at a fixed density or as a function of the density (or hole doping) at a fixed temperature. In Fig. 1 we plot the hole density as a function of the temperature for different chemical potentials. The results of the bare NLC sums (3) exhibit a clear feature. They converge to lower temperatures as the density approaches 1.

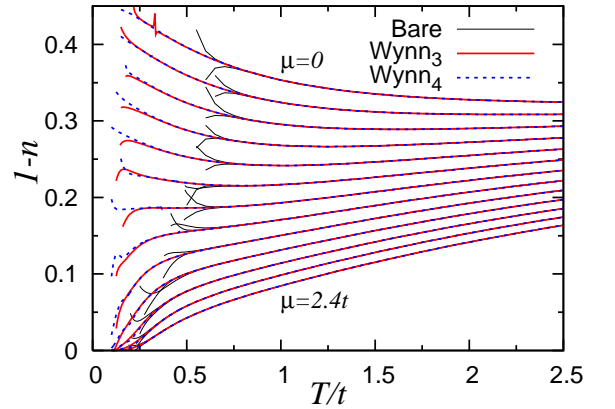


FIG. 1: (Color online) Hole density as a function of temperature for different chemical potentials (from top to bottom  $\mu = 0, 0.2, \dots, 2.4$ ), and  $J/t = 0.5$ . For each value of the chemical potential we have plotted results of the bare NLC sums up to 9 and 10 sites (thin continuous lines) and results of Wynn extrapolations after three and four cycles of improvement (see Ref. [2] for details).

In order to access lower temperatures we use the sequence extrapolation techniques detailed in Ref. [2]. Results of Wynn extrapolations for the density after three

and four cycles of improvement are also depicted in Fig. 1. For the lowest chemical potential ( $\mu = 0$ ) one can see that series extrapolations allow one to extend the region of convergence of the density from  $T/t > 0.75$  to  $T/t < 0.2$ .

Once we have performed the extrapolations for the density, we numerically invert the dependence of any observable from  $(\mu, T)$  to  $(n, T)$ . As a first example we show in Fig. 2 the dependence of the chemical potential on the temperature when the density is held fixed. As can be seen, it is possible to follow the chemical potential curves at constant density to rather low temperatures  $T/t \sim 0.1$ .

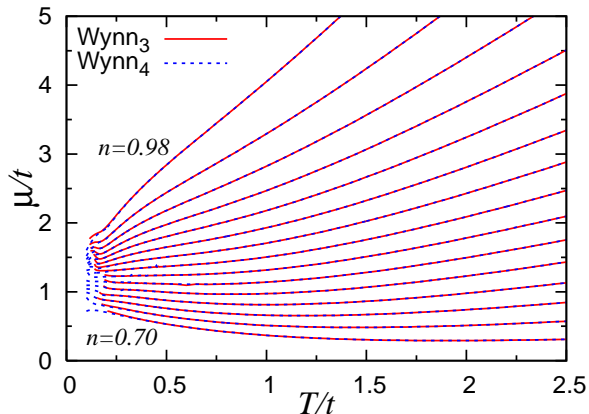


FIG. 2: (Color online) Chemical potential as a function of temperature for different densities (from bottom to top  $n = 0.7, 0.72, \dots, 0.98$ ), and  $J/t = 0.5$ . For each value of the density we have plotted results of Wynn extrapolations after three and four cycles of improvement.

An analysis of the results depicted in Fig. 2 for the lowest temperatures suggests that the dependence of  $\mu$  on the temperature is roughly linear

$$\mu(T) = \mu(T = 0) + A T. \quad (7)$$

This is in agreement with the results obtained by JP [8] using FTLM, and departs from the  $T^2$  dependence expected of a Fermi liquid. In addition, there is a change in the slope  $A$  as the density is shifted. For  $J/t = 0.5$  we find that the slope  $A$  changes sign when  $n' \sim 0.81$ . This can be better seen in Fig. 3, where we plot the hole density vs the chemical potential at fixed temperatures. There, one can see that for  $1 - n' \sim 0.19$  the different curves cross each other. For  $1 - n' < 0.19$  our NLC results are well converged at all temperatures  $T/t > 0.15$ . Small departures between Wynn extrapolations after three and four cycles of improvement are only apparent for the lowest temperatures and highest hole concentrations.

We have also performed a similar study for  $J/t = 0.3$ . In this case we have obtained, in close agreement with JP [8], that the change of slope in  $A$  occurs for  $n' \sim 0.86$ .

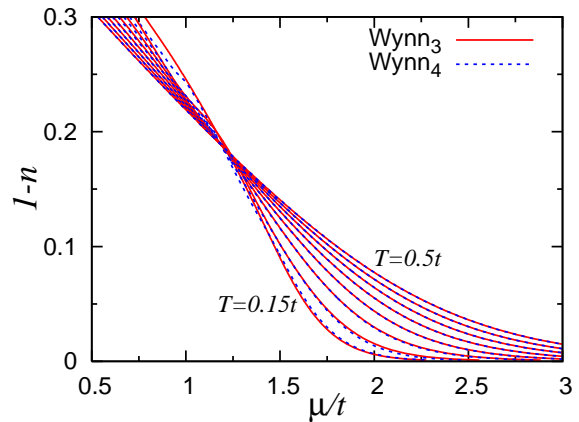


FIG. 3: (Color online) Hole density vs chemical potential for different temperatures (below the crossing point from bottom to top  $T/t = 0.15, 0.20, \dots, 0.5$ ), and  $J/t = 0.5$ . For each value of the temperature we have plotted results of Wynn extrapolations after three and four cycles of improvement.

### III. ENTROPY

Once one has numerically inverted the dependence  $(\mu, T)$  to  $(n, T)$  it is possible to study the behavior of observables of interest as a function of the temperature at a fixed density. In this section we consider the entropy per lattice site

$$S = \frac{1}{N} \left( \ln Z + \frac{\langle \mathcal{H} - \mu \sum_i n_i \rangle}{T} \right), \quad (8)$$

where the term proportional to the chemical potential on the right hand side, not present in our calculations for spin systems, is needed when dealing with the grand canonical ensemble.  $N$  is the number of lattice sites.

In Fig. 4, we plot the entropy vs temperature for different values of the density after three and four cycles of improvements using Wynn's algorithm. As with the chemical potential, the NLC convergence for  $S$  improves as the density approaches 1. For all the densities plotted in Fig. 4 we get good convergence for  $T/t \geq 0.25$ .

Now we discuss the dependence of the entropy on density when the temperature is held fixed. This is shown in Fig. 5. The entropy exhibits a very broad maximum that slowly shifts towards lower hole densities as the temperature is increased. These results are in qualitative agreement with experimental measurements that have found the entropy to be maximum around  $1 - n = 0.22$  at a temperature  $T/t = 0.07$  (lower than the ones we have calculated here) [19].

To conclude this section on the entropy we compare in Fig. 6 our NLC results with those obtained by JP [8] using FTLM in clusters with 20 lattice sites and  $J/t = 0.3$ . At zero doping (Heisenberg model), the agreement between NLC (with clusters up to 13 sites [1]) and FTLM is remarkable down to  $T/t \sim 0.25$ . Below that temperature, finite size effects start to be apparent as FTLM results marginally depart from the ones obtained using

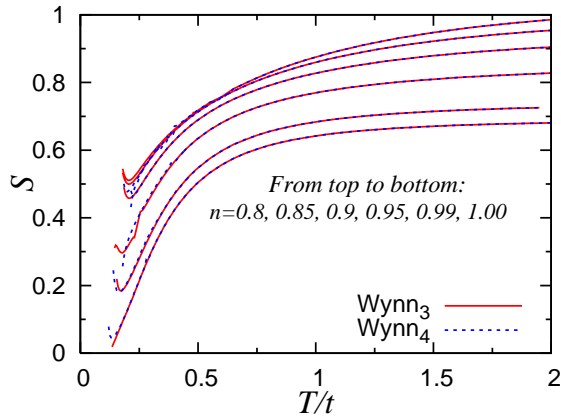


FIG. 4: (Color online) Entropy as a function of temperature for different densities and  $J/t = 0.5$ . For each value of the density we have plotted results of Wynn extrapolations after three and four cycles of improvement.

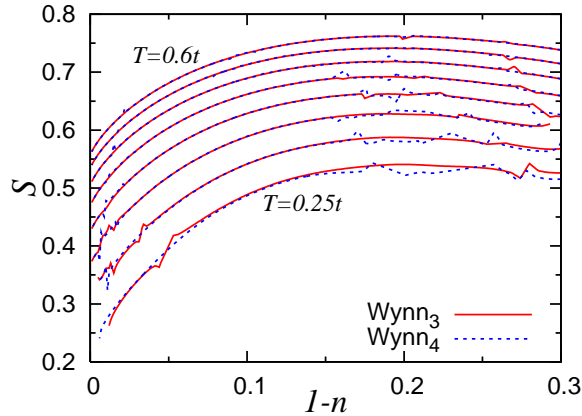


FIG. 5: (Color online) Entropy as a function of the density for different temperatures (from bottom to top  $T/t = 0.25, 0.20, \dots, 0.6$ ) and  $J/t = 0.5$ . For each value of the temperature we have plotted results of Wynn extrapolations after three and four cycles of improvement.

NLC (see also discussion in Ref. [1] on the entropy of the Heisenberg model on the square lattice).

Within FTLM, finite size effects for the entropy, at a given temperature, increase when holes are added to the antiferromagnet. This can be understood within the analysis presented in Ref. [8]. There it was shown that the temperature at which finite size effects start to become relevant increases with doping  $1 - n \gtrsim 0.15$ , for the system sizes considered in that work. In particular, for  $n = 0.7$  (the worst case for FTLM) our NLC results for  $S$  are slightly different from the ones in Ref. [8] for all temperatures in Fig. 6.

#### IV. UNIFORM SUSCEPTIBILITY

We study in this section another thermodynamic quantity of much experimental interest, the uniform suscepti-

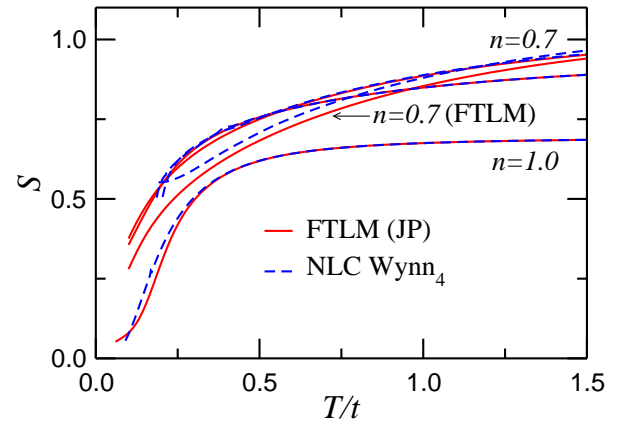


FIG. 6: (Color online) Entropy as a function of temperature for different densities (from top to bottom at  $T/t = 1.5$  NLC results correspond to  $n = 0.7, 0.8, 0.9$ , and  $1.0$ ) and  $J/t = 0.3$ . Our Wynn extrapolations after four cycles of improvement are compared with FTLM results by JP [8].

bility

$$\chi = \frac{\langle (S_{\text{tot}}^z)^2 \rangle}{NT}. \quad (9)$$

In Fig. 7 we show results for the uniform susceptibility as a function of temperature for different densities. For the Heisenberg model, the results of our Wynn extrapolations for  $\chi$  are well converged down to  $T/J \sim 0.3$ . They allow one to resolve the peak in  $\chi$  that occurs around  $T/J \sim 1$ , and signals the onset of short range antiferromagnetic order. With doping the peak shifts to lower temperatures, i.e., the doping slows down the growth of antiferromagnetic correlations, and eventually disappears. Only for  $n = 0.9$  and  $0.95$  do our NLC results exhibit signals of a peak in  $\chi$ .

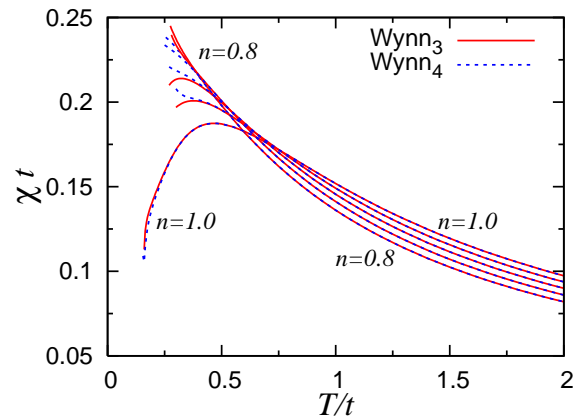


FIG. 7: (Color online) Uniform susceptibility as a function of the temperature for different densities (from bottom to top for the highest temperatures  $n = 0.8, 0.85, \dots, 1.0$ ) and  $J/t = 0.5$ . For each value of the density we have plotted results of Wynn extrapolations after three and four cycles of improvement.

In what follows we compare NLC results for the uniform susceptibility with the ones obtained using HTE [13]. We first contrast, in Fig. 8, the results of the NLC bare sums (3) for the bond and site expansions with those obtained for the HTE bare sums up to order 10. Figure 8 shows that the direct NLC sums converge down to  $T/t \sim 0.75$  (with the site expansion being slightly better than the bond expansion), while the HTE results are only well converged to  $T/t \sim 1.25$ . The existence of this region of temperatures where NLC converges while HTE does not was our main motivation for developing NLC, and makes NLC a more controlled technique at intermediate temperatures.

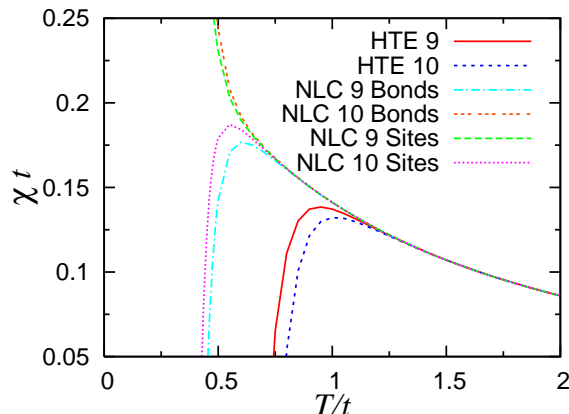


FIG. 8: (Color online) Uniform susceptibility results for the bare NLC sums of the bond and site expansions compared with those obtained with HTE up to order 10. The density in the system is  $n = 0.85$ .

As discussed before, an important feature of NLC and HTE is that both approaches allow for systematic extrapolations that accelerate the convergence of NLC and enable going beyond the radius of convergence of HTE. In Fig. 9 we compare Pade extrapolations for  $\chi$  with Wynn extrapolations for the NLC site expansion. The agreement between these two approaches is remarkable down to  $T/t \sim 0.5$ , which show that indeed extrapolations can work quite well for both techniques, if the temperature is not too low. For this quantity, however, different Wynn extrapolations converge to lower temperatures than the Pade approximants. We find this to be remarkable for itinerant models because the analytic structure of HTE allows for an analytic inversion of the grand-canonical  $(\mu, T)$  dependence into the more experimentally relevant one  $(n, T)$ . Within NLC we have to perform a numerical extrapolation to access lower temperatures and then do a numerical inversion  $(\mu, T) \rightarrow (n, T)$ . Still, the fact that NLC contains exact information from the finite clusters at all temperatures, while in HTE only a power series expansion in inverse temperature is kept, means that the former, in a real sense, requires less extrapolation.

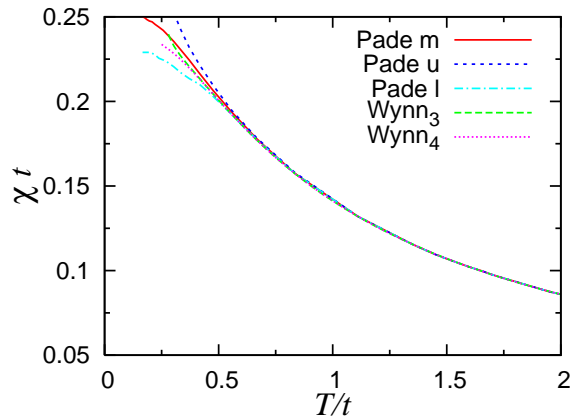


FIG. 9: (Color online) Pade approximants for the uniform susceptibility [13] are compared with Wynn extrapolations of the NLC site expansion. In the legend, Pade m, Pade u, and Pade l, indicate the mean estimated value, upper, and lower limits, respectively, obtained by different Pade approximants. The density in the system is  $n = 0.85$ .

## V. SPECIFIC HEAT

In this section we analyze the NLC results for the specific heat and compare them with those obtained within FTLN [8]. The specific heat is defined as

$$C_v = T \left( \frac{\partial S}{\partial T} \right)_{N_e}. \quad (10)$$

However, we avoid the numerical differentiation of the entropy with respect to the temperature by evaluating

$$C_v = \frac{\langle \mathcal{H}^2 \rangle - \langle \mathcal{H} \rangle^2}{NT^2} - \frac{1}{NT} \left( \frac{\partial N_e}{\partial \mu} \right)_T \left\{ \left( \frac{\partial \langle \mathcal{H} \rangle}{\partial N_e} \right)_T \right\}^2, \quad (11)$$

which substantially reduces the numerical errors as the NLC sums for the number of particles ( $N_e = \langle \sum_i n_i \rangle$ ) and the energy ( $\langle \mathcal{H} \rangle$ ) converge (and are better behaved) to lower temperatures than the ones of the entropy. Still, we have to perform numerical derivatives in addition to calculating the fluctuations of the energy ( $\langle \mathcal{H}^2 \rangle - \langle \mathcal{H} \rangle^2$ ). Hence, of the thermodynamic observables analyzed so far  $C_v$  is the most difficult for NLC evaluation.

In Fig. 10 we plot the specific heat as a function of the temperature for different densities. For  $C_v$  we only obtain well converged results below  $T/t = 0.5$  for the Heisenberg model and the  $t$ - $J$  model at low hole concentration. Figure 10 shows that the maximum in the specific heat, attributed to the thermal activation of the spin degrees of freedom, becomes strongly suppressed with doping. This can be better seen in Fig. 11, where we have plotted the specific heat as a function of the hole density for fixed values of the temperature. For the lowest temperatures in that figure, we only can follow the  $C_v$  curves for doping below 0.15. They clearly show that  $C_v$  decreases as the doping is increased, and exhibits a minimum that moves towards higher doping concentrations as the temperature is lowered.



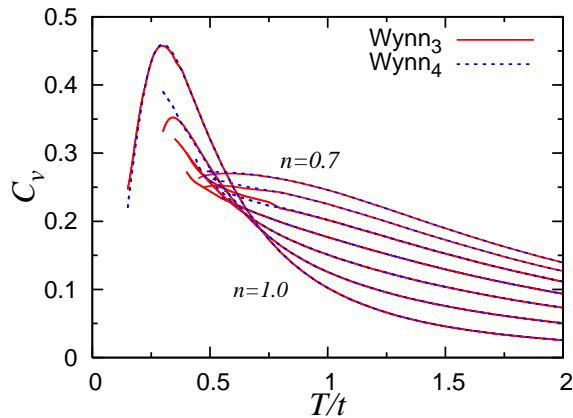


FIG. 10: (Color online) Specific heat as a function of the temperature for different densities (from top to bottom  $n = 0.7, 0.75, \dots, 1.0$ ) and  $J/t = 0.5$ . For each value of the density we have plotted results of Wynn extrapolations after three and four cycles of improvement.

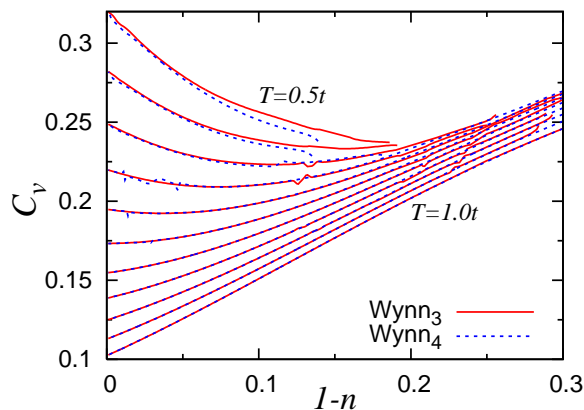


FIG. 11: (Color online) Specific heat as a function of the hole density for different temperatures (from top to bottom  $n = 0.5, 0.55, \dots, 1.0$ ) and  $J/t = 0.5$ . For each value of the temperature we have plotted results of Wynn extrapolations after three and four cycles of improvement.

In Ref. [2] we have argued that the specific heat of the Heisenberg model suffers from large finite size effects at relatively high temperatures. (We presented results for the full diagonalization of a  $4 \times 4$  lattice.) In Fig. 12 we compare our NLC results for the  $t$ - $J$  model with the ones obtained by JP for clusters with 20 lattice sites and  $J/t = 0.3$ . At high temperatures  $T/t > 0.75$  our NLC results are in very good agreement with the ones of JP. NLC results for  $C_v$ , however, do not converge below  $T = 0.5$  when the doping in the system is large. As the density approaches 1, and the convergence of NLC moves to lower temperatures, our linked-cluster results start to depart from the ones obtained with FTLN. In general, we find our calculation of the specific heat in the thermodynamic limit to be below the FTLN results for finite clusters. This deviation becomes particularly large for the Heisenberg model. The FTLN peak for  $C_v$  when  $N = 20$  occurs at larger temperatures than the one ob-

tained within NLC. Interestingly, increasing the system size up to  $N = 26$  does not help since the peak remains at the same position while becoming higher [8], instead of moving to lower temperatures and becoming smaller as has been found to be the case in the thermodynamic limit [2, 20]. This suggests that in general, specific heat is a more difficult quantity to calculate numerically.

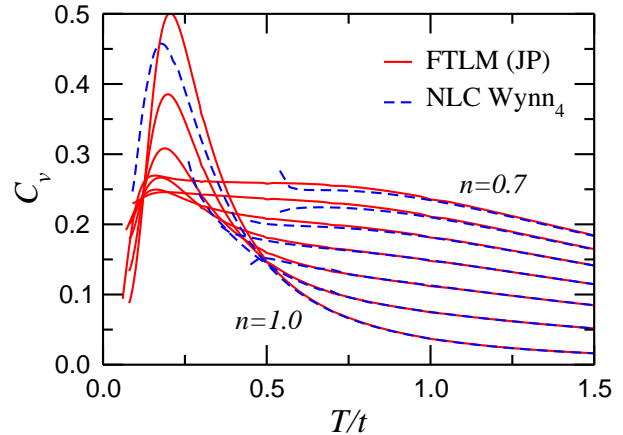


FIG. 12: (Color online) Specific heat as a function of the temperature for different densities (from top to bottom  $n = 0.7, 0.75, \dots, 1.0$ ) and  $J/t = 0.3$ . Our Wynn extrapolations after four cycles of improvement are compared with FTLN results by JP [8].

## VI. CONCLUSIONS

We have presented an application of the recently introduced NLC approach to itinerant models. In particular, we have studied thermodynamic properties of the  $t$ - $J$  model on the square lattice.

From the possible NLC expansions discussed in Ref. [2], we have found that the one best suited to the  $t$ - $J$  model on the square lattice is the site based expansion. For this expansion we have shown that the NLC bare sums (for the observables considered here) converge to lower temperatures than the bare HTE sums. In addition, Wynn extrapolations for the site based expansion were found to provide better results at lower temperatures than the ones obtained with Pade extrapolations for HTE. This in spite of the fact that the inversion of the dependence  $(\mu, T)$  to  $(n, T)$  can be done analytically within HTE, while within NLC it is done numerically.

Through a comparison with results obtained by Jaklič and Prelovšek using the finite-temperature Lanczos method [8, 11], we have also shown that NLC allows one to access regions at low temperatures where finite size effects are relevant to exact diagonalization studies. One particularly striking example presented here is the peak in the specific heat of the Heisenberg model. In the calculations done in Refs. [8, 11] it was found that with increasing the system size (within the sizes that can be addressed by exact diagonalization) the peak does not

move while it does increase in size. NLC results, which confirmed previous results by Bernu and Misguich [20], exhibit a smaller peak shifted towards lower temperatures.

Moving away from Heisenberg models, it remains to be seen as to which method is in general accurate to lower temperatures. Future application of NLC to superconducting and other exotic susceptibilities should prove informative. The study of the former using HTE remains controversial [21, 22, 23]. It may also prove useful to combine NLC with Lanczos and FTLM methods to extend

it to still lower temperatures.

### Acknowledgments

This work was supported by the US National Science Foundation, Grant Nos. DMR-0240918, DMR-0312261, and PHY-0301052. We are grateful to P. Prelovšek for providing us with the data from Ref. [8], and for useful comments on FTLM.

- 
- [1] M. Rigol, T. Bryant, and R. R. P. Singh, Phys. Rev. Lett. **97**, 187202 (2006).
  - [2] M. Rigol, T. Bryant, and R. R. P. Singh, Phys. Rev. E (2006).
  - [3] P. W. Anderson, Science **235**, 1196 (1987); G. Baskaran, Z. Zou, and P. W. Anderson, Solid State Commun. **63**, 973 (1987).
  - [4] F. C. Zhang and T. M. Rice, Phys. Rev. B **37**, 3759 (1988).
  - [5] G. J. Bednorz and K. A. Müller, Z. Phys. B **64**, 188 (1986).
  - [6] M. K. Wu, J. R. Ashburn, C. J. Torng, P. H. Hor, R. L. Meng, L. Gao, Z. J. Huang, Y. Q. Wang, and C. W. Chu, Phys. Rev. Lett. **58**, 908 (1987).
  - [7] S. Chakravarty, R. B. Laughlin, D. K. Morr, and C. Nayak, Phys. Rev. B **63**, 094503 (2001).
  - [8] J. Jaklič and P. Prelovšek, Adv. Phys. **49**, 1 (2000).
  - [9] A. Sokol, E. Gagliano, and S. Bacci, Phys. Rev. B **47**, 14646 (1993).
  - [10] H. Tsunetsugu and M. Imada, J. Phys. Soc. Jpn. **66**, 1876 (1997).
  - [11] J. Jaklič and P. Prelovšek, Phys. Rev. B **49**, 5065 (1994).
  - [12] W. O. Putikka, M. U. Luchini, and T. M. Rice, Phys. Rev. Lett. **68**, 538 (1992).
  - [13] R. R. P. Singh, and R. L. Glenister, Phys. Rev. B **46**, 11871 (1992); **46**, 14313 (1992).
  - [14] B. S. Shastry, B. I. Shraiman, and R. R. P. Singh, Phys. Rev. Lett. **70**, 2004 (1993).
  - [15] W. O. Putikka, R. L. Glenister, R. R. P. Singh, and H. Tsunetsugu, Phys. Rev. Lett. **73**, 170 (1994).
  - [16] For a general introduction see C. Domb and M. S. Green, *Phase Transitions and Critical Phenomena*, (Academic Press, New York, 1974), Vol. 3.
  - [17] J. Oitmaa, C. Hamer, and W-H. Zheng, *Series Expansion Methods for Strongly Interacting Lattice Models* (Cambridge University Press, Cambridge, 2006).
  - [18] A. J. Guttmann, in *Phase Transitions and Critical Phenomena*, edited by C. Domb and J. Lebowitz (Academic Press, London, 1989), Vol. 13.
  - [19] J. M. Loram, K. A. Mirza, J. R. Cooper, N. A. Athanasopoulou, and W. Y. Liang, *Proceedings of the 10<sup>th</sup> Anniversary HTS Workshop, Houston*, (World Scientific, Singapore, 1996), p. 341.
  - [20] B. Bernu and G. Misguich, Phys. Rev. B **63**, 134409 (2001).
  - [21] L. P. Pryadko, S. A. Kivelson, and O. Zachar, Phys. Rev. Lett. **92**, 067002 (2004).
  - [22] T. Korestune and M. Ogata, J. Phys. Soc. Jpn. **74**, 1390, (2005).
  - [23] W. O. Putikka and M. U. Luchini, Phys. Rev. Lett. **96**, 247001 (2006).